

ADP-AT-97-1
Astroparticle Physics, submitted

Gamma-Rays and Neutrinos from Very Young Supernova Remnants

R.J. Protheroe, W. Bednarek*, and Q. Luo

Department of Physics and Mathematical Physics
 The University of Adelaide, Adelaide, Australia 5005
 *permanent address: University of Łódź, 90-236 Łódź,
 ul. Pomorska 149/153, Poland.

Abstract

We consider the result of acceleration of heavy ions in the slot gap potential of a very young pulsar with a hot polar cap. Photodisintegration of the heavy ions in the radiation field of the polar cap and pulsar surface gives rise to a flux of energetic neutrons. Some fraction of these neutrons interact with target nuclei in the supernova shell to produce a prompt neutrino and gamma-ray signal. Neutrons that do not interact promptly travel far from the pulsar where they decay into protons which await the arrival of target nuclei in the supernova shell, and then produce a delayed neutrino and gamma-ray signal. The TeV neutrino and 100 MeV and TeV gamma-ray signals should be observable from very young supernova remnants in our galaxy for a range of pulsar parameters.

1 Introduction

Young supernova remnants are probably sites of acceleration of particles to high energies and, as a result of interactions, also sources of high energy neutrinos and γ -rays [1–6]. Following the occurrence of SN1987A it was expected that high energy γ -rays would be detected from this object, but the observations have so far been negative [7–14]. Also, some models required the formation of a pulsar during the supernova (SN) explosion which has not yet been discovered. Nevertheless, SN1987A renewed interest in predicting neutrino and γ -ray fluxes from supernova remnants (SNR) for times soon after the explosion. For example, the model in which protons are accelerated at the reverse shock which forms in a relativistic wind from a pulsar as a result of its confinement by the supernova envelope, proposed by Rees & Gunn [15], has been considered in several papers [4, 5, 16, 17]. In this model, relativistic protons produce γ -rays and neutrinos in

collisions with the matter in the shell, and observable γ -ray fluxes were predicted for SN 1987A if the power in relativistic protons was $\sim 10^{39}$ erg s $^{-1}$. If the pre-supernova star had a strong wind, neutrinos and γ -rays could be produced in collisions of relativistic particles accelerated by the supernova shock itself, with the surrounding matter. For this scenario, Kirk et al. [18] predicted detectable fluxes of TeV γ -rays for SN 1993J, but not for SN 1987A.

In the present paper, we consider yet another scenario in which particle acceleration along open magnetic field lines may take place in the pulsar magnetosphere if a neutron star with a high magnetic field and a sufficiently short period forms during the supernova explosion. That acceleration of heavy ions by the Crab pulsar may take place, has already been suggested, based on modelling the observed synchrotron wisps in the Crab nebula [19, 20]. In these papers it is proposed that $\sim 2/3$ of the rotational kinetic energy loss of the Crab pulsar is carried by ions which are injected with a rate close to the Goldreich & Julian current, and that these ions are accelerated through at least 20% of the total voltage available on open field lines.

It is expected that soon after supernova explosions the surface temperatures of resulting neutron stars are much higher than derived from recent observations of the thermal emission from the surfaces of classical pulsars [21–23]. Just after formation, a neutron star’s surface temperature is very high ($\sim 10^{11}$ K) but drops very rapidly, and models of neutron star cooling predict temperatures of the order of a few 10^6 – 10^7 K during the first ~ 10 years after the explosion [24, 25]. However, the polar cap of a neutron star can have a temperature $\sim 10^7$ K or higher, due to the heating by electrons and γ -rays from cascades in the pulsar magnetosphere [26–28], and their thermal emission depends only on the pulsar parameters.

Nuclei, probably mainly Fe nuclei, extracted from the neutron star surface and accelerated to high Lorentz factors can be photodisintegrated during propagation through the neutron star’s radiation field. Relativistic neutrons extracted from Fe nuclei in this way propagate straight out and escape from the magnetosphere, interacting in or passing through the surrounding supernova remnant shell. Those interacting in the shell produce what we shall refer to as the “prompt flux” of neutrinos and γ -rays. Those passing through the shell decay into relativistic protons which are trapped and isotropized by the ambient magnetic field. These protons wait for the matter target, i.e. the supernova shell, to catch up with them. As the SNR shell expands, it interacts with these accumulated energetic protons from neutron decay, producing what we shall refer to as the “delayed flux” of neutrinos and γ -rays.

In Sect. 2 we investigate the photodisintegration of nuclei in the radiation field of a pulsar. In Sect. 3 we consider the energetics of pulsars and the acceleration of particles in the slot gap, as well as polar cap heating. We then compute in Sect. 4 the spectrum of neutrons escaping from the pulsar’s radiation field, and in Sect. 5 the expected light curves and spectra of γ -rays and neutrinos. The acceleration of Fe nuclei in the outer gap of classical radio pulsars [29, 30], and photodisintegration of Fe on the nonthermal radiation of the outer gap will be considered in a future paper [31].

2 Photodisintegration of nuclei in pulsar thermal radiation

The possibility of photodisintegration of Fe nuclei during their propagation through thermal radiation from very young neutron stars has been noted by Bednarek & Karakuła [32]. The importance of this process can be evaluated by calculating the mean free path, $\lambda_A(\gamma_A, T)$, for relativistic nuclei with mass number A and Lorentz factor γ_A for photodisintegration, typically of one nucleon, in black body radiation with temperature T which is given by

$$\frac{1}{\lambda_A(\gamma_A, T)} = \int \int \frac{\epsilon^* n(\epsilon, T) \sigma_A(\epsilon^*)}{2\gamma_A \epsilon} d\epsilon d(\cos \theta), \quad (1)$$

where $n(\epsilon, T)$ is the photon number density per unit photon energy at photon energy ϵ for black body radiation at temperature T , $\sigma_A(\epsilon^*)$ is the cross section for photodissociation of a single nucleon from a nucleus with mass number A [33], $\epsilon^* = \gamma_A \epsilon (1 - \beta_A \cos \theta)$ is the photon energy in the rest frame of the nucleus, β_A is the velocity of the nucleus, and θ is the angle between the direction of the nucleus and a thermal photon. In Fig. 1 we show the mean free paths for isotropic black body radiation with temperature T , for nuclei with various mass numbers as a function of Lorentz factor. Note that the mean free paths computed by us using Eq. 1 differ slightly for low A nuclei in comparison with those given by Karakuła & Tkaczyk [33] because the cross section given by Eq. 2 of their paper incorrectly separates the contributions from the Breit-Wigner peak and the approximately constant cross section at high energies.

To check if photodisintegration of Fe nuclei propagating in the anisotropic radiation field of a neutron star perpendicular to its surface is important, we compute the average number of neutrons extracted from Fe nuclei as a function of their Lorentz factor γ_{Fe} . We have made the reasonable approximation, that in every photodisintegration, only one nucleon is extracted. In Fig. 2(a) we show the average number of neutrons extracted from Fe nuclei as a function of Lorentz factor γ_{Fe} for different surface temperatures. It is clear that for a neutron star with a uniform surface temperature, the temperature needs to be rather high, above $\sim 10^7$ K, for the process to occur efficiently. Such surface temperatures are higher than expected except within a few days of the explosion. However, as we shall discuss in the next section, neutron star polar caps may have very high temperatures due to particle acceleration and cascading in the magnetosphere. We show in Fig. 2(b) the average number of neutrons extracted from Fe nuclei as a function of Lorentz factor in the radiation field of a heated polar cap of radius 10^5 cm for three temperatures, and we see that efficient photodisintegration can take place in such a radiation field.

3 Pulsar energetics and particle acceleration

We are interested in the case of a very young pulsar which has just been formed during a supernova explosion, and for a few years after formation. It is assumed that pulsar

acceleration can operate very soon after the formation of a neutron star and can tap into a substantial fraction of the spin-down power that is not associated with gravitational radiation. We approximate this non-gravitational component of the spin-down power by the magnetic dipole radiation power (erg s⁻¹) given by

$$L_{\text{em}}(\Omega, B) = B^2 R^6 \Omega^4 \sin^2 i / 6c^3, \quad (2)$$

where B is the surface magnetic field at the magnetic pole in G, R is the radius of the neutron star in cm, $\Omega = 2\pi/P$ where P is the period in s, and i is the angle between the spin axis and rotation axis.

For acceleration of ions up to sufficiently high energies for photodisintegration to take place we need to have both a short initial period and a high magnetic field. Thus, in all the calculations we make in the present paper we shall adopt $B \sin i = 10^{13}$ G, and an initial period of either $P_0 = 2$ ms or $P_0 = 5$ ms. Our results will therefore only apply directly to a subset of pulsars with high magnetic fields and short initial periods which would therefore have favourable conditions for particle acceleration. The magnetic field we adopt is comparable with those inferred to be present in some pulsars. Equating L_{em} with the loss of rotational kinetic energy, and taking $R = 1.2 \times 10^6$ cm and moment of inertia $I = 1.4 \times 10^{45}$ g cm² (see e.g. Shapiro & Teukolsky [34]), one obtains

$$B \sin i \cong 7.6 \times 10^{19} (P \dot{P})^{1/2} \quad \text{G.} \quad (3)$$

Using this formula, and data taken from Taylor, Manchester & Lyne [35], we find that a number of pulsars have $B \sin i$ above 10^{13} G (e.g. PSR 150–58 – 3.7×10^{13} G; PSR 1916+14 – 3.7×10^{13} G; PSR 1737-30 – 3.9×10^{13} G)

Equating L_{em} with the loss of rotational kinetic energy, the period at time t is given by the well-known formula,

$$P^2(t) = 1.04 \times 10^{-15} t B_{12}^2 \sin^2 i + P_0^2, \quad (4)$$

where $B = 10^{12} B_{12}$ G, P_0 is the initial pulsar period in seconds, and we have again used $R = 1.2 \times 10^6$ cm and $I = 1.4 \times 10^{45}$ g cm². Note that Eq. 4 neglects other sources of loss of rotational kinetic energy, e.g. by gravitational radiation or electromagnetic quadrupole radiation (see the discussion by Manchester and Taylor [36]). The electromagnetic quadrupole radiation which might be important in very young pulsars is very uncertain and we shall neglect this. However, gravitational radiation losses are known to be important for very young pulsars and the power in gravitational radiation (erg s⁻¹) is given by

$$L_{\text{gr}}(\Omega, k) = -\frac{32}{5} \frac{G_N}{c^5} I^2 k^2 \Omega^6 \quad (5)$$

where G_N is the gravitational constant, I is the moment of inertia and k is the ellipticity [34]. We adopt $k = 3 \times 10^{-4}$ which is required in the case of the Crab pulsar to give

a pulsar age equal to the time elapsed since the observation of the Crab supernova in 1054 [34].

Starting with an initial pulsar period we have performed numerical integrations over pulsar age to obtain the period as a function of age for the case where both electromagnetic losses and gravitational radiation losses are included. We show in Fig. 3 the period as a function of age for $B \sin i = 10^{13}$ G and $k = 3 \times 10^{-4}$ for two initial periods: $P_0 = 2$ ms and $P_0 = 5$ ms.

According to standard models of neutron star cooling, the surface temperature decreases to $T \sim 10^7$ K at a few days after the explosion, and later cools much more slowly, reaching $T \sim 4 \times 10^6$ K in one year. In our calculations, we interpolate between the results of Nomoto and Tsuruta [24] for which $\log(T/1 \text{ K})$ is 6.99, 6.72, 6.58, and 6.55 at $\log(t/1 \text{ y}) = -2, -0.94, 0.08$, and 1.11 respectively.

Models of high energy processes in pulsars predict polar cap temperatures can be significantly higher because of the heating caused the relativistic e^\pm pairs and γ -rays created in the gaps in the pulsar magnetosphere. For the space charge limited flow model [27, 40, 41] a lower limit on the polar cap temperature can be estimated

$$T_c^{AS} \approx 2.6 \times 10^5 P^{-19/32} B_{12}^{1/4} R_6^{5/16} \text{ K}, \quad (6)$$

where P is in seconds and $R = 10^6 R_6$ cm. In deriving this formula it is assumed that the heating rate (given by Eq. 75 in Arons & Scharlemann [27]) applies to the region of the polar cap defined by the last open field line which intersects the pulsar surface at $(r, \theta) = (R, \theta_c)$ where

$$\theta_c \approx (\Omega R/c)^{1/2} \quad (7)$$

giving a polar cap radius of

$$r_c \approx (2\pi^3/cP)^{-1/2}. \quad (8)$$

Arons & Scharlemann [27] note that the heating rate may actually be even higher, as given by the model of Ruderman & Sutherland [26], if most of e^\pm pairs created in the polar gap can be reversed and fall on the polar cap region. The Ruderman & Sutherland heating rate (given by Eq. 26 in their paper) defines an upper limit to the polar cap temperature

$$T_c^{RS} \approx 2.8 \times 10^6 P^{-8/28} B_{12}^{6/28} R_6^{-17/28} \text{ K}. \quad (9)$$

Note that in both models the polar cap temperatures depends on the pulsar parameters. For very rapid pulsars with high magnetic fields they can reach $\sim 10^7$ K or higher. In the present paper we shall refer to the Arons & Scharlemann model (Eq. 6) as “moderate polar cap heating” and the Ruderman & Sutherland model (Eq. 9) as “maximum polar cap heating”.

For hot polar caps, thermionic emission of ions is allowed, and because of the free supply of charges from the polar caps, the rotation-induced potential should be space

charge limited (e.g. refs. [27, 37, 38]). Whether ions or electrons are accelerated out along field lines depends on the sign of the accelerating electric field. Here we consider only the case in which ions are accelerated.

It is usually assumed that the pulsar surface is composed largely of highly ionized Fe although other compositions, e.g. He nuclei [39], are also possible. Here, we assume that the all the outflowing ions are fully-ionized Fe (e.g. [38]). Fe nuclei accelerated in the magnetosphere may reach sufficiently high Lorentz factors such that photodisintegration could occur efficiently. To gain an impression about the pulsar parameters for which this may be important, we assume particles are accelerated by the electric field in the slot gap [27, 40, 41]. In this model the electric potential in the gap is given approximately by

$$\Phi(x) \approx 0.375\theta_c^4 B R g(x) \eta(1 - \eta^2) \sin \zeta \sin i \quad \text{V}, \quad (10)$$

where η is the ratio of the colatitude angle of the open field lines to θ_c , and ζ is the azimuthal angle with respect to the magnetic pole. In the equation, $g(x) \approx x^2$ for $x < 0.5\theta_c$, and $g(x) \approx \theta_c[(x + 1)^{0.5} - 1]$ for $x > 0.5\theta_c$, and x is the distance along the gap in units of R . In writing Eq. 10, we ignore the terms due to the complicated geometry of the gap. The ion acceleration zone corresponds to $\zeta > \pi/2$. We shall adopt $\eta = 0.1$ and $\zeta = 3\pi/2$ in our work. This potential is shown in Fig. 4 for $B \sin i = 10^{13}$ G and for periods equal to the two initial periods, i.e. $P = 0.002$ s and $P = 0.005$ s.

4 Spectrum of neutrons from photodisintegration of Fe nuclei

The extraction of energetic neutrons from accelerated nuclei has important consequences for the transport of energy from the pulsar's vicinity to the nebula since they move ballistically through the magnetosphere and beyond the light cylinder. Their Lorentz factors are approximately equal to the Lorentz factors of the parent nuclei, and are sufficiently high that they typically decay at large distances from the pulsar. Initially the SNR shell is opaque to neutrons so that most neutrons interact in the dense shell. Later, when the shell becomes transparent to neutrons, they move through the SNR shell and decay outside it. Most of the energy of the neutrons is then taken by protons which are trapped and isotropized by the ambient magnetic field, and these protons then wait for target nuclei, i.e. the SNR shell, to arrive. When the SNR shell catches up with the relativistic protons, production of γ -rays and neutrinos occurs through hadronic collisions.

The dependence of the electric potential in the case of the slot gap model as a function of distance (Eq. 10) defines the Lorentz factor of Fe nuclei during their propagation from the surface. Using this potential we compute the average number of neutrons extracted from Fe nuclei as a function of pulsar age. We show this in Fig. 5(a) for $P_0 = 5$ ms and $P_0 = 2$ ms for each of the following three radiation field models: whole neutron star at a surface temperature which depends on age as given by Nomoto and Tsuruta [24]; surface temperature as before plus hot polar cap which has moderate heating (Eq. 6);

surface temperature as before plus hot polar cap which has maximum heating (Eq. 9). In Fig. 5(b) we show the average cumulative number of neutrons extracted from a single Fe-nucleus during acceleration for $P = 5$ ms and $P = 2$ ms as a function of distance along the slot gap for the three radiation field models.

Since at a particular distance, a neutron extracted from the accelerated ion will have an energy determined by the slot gap potential, we can now compute the energy spectra of neutrons escaping from the pulsar radiation field per single Fe nucleus accelerated. In Fig. 6 we show the spectrum of neutrons extracted from a single Fe-nucleus during acceleration, $N_n(E_n)$, for a pulsar with $P_0 = 5$ ms and $B \sin i = 10^{13}$ G, for the three radiation field models. Results are given for (a) $t = 1.15$ days ($P = 5$ ms), (b) $t = 20.5$ days ($P = 5.06$ ms), and (c) $t = 1$ year ($P = 5.94$ ms). In Fig. 7 we compare the spectrum of neutrons at $t = 1$ year produced for $P_0 = 5$ ms with that produced with $P_0 = 2$ ms.

The differential production rate, $\dot{N}_n(E_n)$, of neutrons extracted from Fe nuclei depends on the total rate of Fe nuclei injected, \dot{N}_{Fe} , and is given by

$$\dot{N}_n(E_n) = \dot{N}_{\text{Fe}} N_n(E_n) = \frac{\xi L_{\text{em}}(\Omega, B)}{Ze\Phi_{\text{max}}(\Omega, B)} N_n(E_n) \quad (11)$$

where $L_{\text{em}}(\Omega, B)$ is the magnetic dipole radiation approximation to the total non-gravitational radiation spin-down power (Eq. 2), $\Phi_{\text{max}}(\Omega, B) = \Phi(r_{\text{LC}}/R)$ is the acceleration potential traversed by Fe nuclei given by Eq. 10 and r_{LC} is the distance to the light cylinder up to which this acceleration is assumed to occur, $Z = 26$ is the atomic number of Fe, and e unit electric charge. The parameter ξ gives the fraction of total pulsar power used to accelerate Fe nuclei and has an upper-limit $\xi \approx \Phi_{\text{max}}/\Phi_0 \approx 0.29$ where $\Phi_0 = 0.5\theta_c^4 BR$ is the maximum potential drop across the polar cap (e.g. Luo et al. [42]). Note that we write the rate of injection of iron nuclei as the ratio of a fraction of the power, ξL_{em} to the maximum particle energy, $Ze\Phi_{\text{max}}$ since the ratio gives the same order-magnitude estimate of the injection rate as that derived from Goldreich-Julian density.

5 Gamma-ray and neutrino spectra

We make the approximation that the SNR shell has a thickness which is much smaller than the radius of the shell, r_{SN} . The optical depth of the shell to nucleon-nucleon collisions is then

$$\tau_{pp} = M_{\text{SN}} \sigma_{pp} / (4\pi r_{\text{SN}}^2 m_p) \approx 3.5 \times 10^{-5} M_{10} / (\beta_{\text{SN}} t_y)^2 \quad (12)$$

where $M_{\text{SN}} = 10M_{10}$ M $_{\odot}$ is the mass ejected into the shell during the explosion, $\sigma_{pp} \approx 3 \times 10^{-26}$ cm 2 is the proton-proton inelastic cross section, m_p is the proton mass, $t = t_y$ years is the time after the explosion, and $v_{\text{SN}} = \beta_{\text{SN}} c$ is the shell expansion velocity. Initially the shell is optically thick. For example, if $M_{\text{SN}} = 10M_{\odot}$ and $\beta_{\text{SN}} = 0.03$ the optical depth is greater than 1 for $t < 2$ months. All the results we shall present below are for $\beta_{\text{SN}} = 0.03$ and $M_{\text{SN}} = 10$ M $_{\odot}$.

5.1 Prompt gamma-ray and neutrino spectra

During the early phase most of the neutrons interact with matter in the shell producing prompt γ -ray and neutrino fluxes. These signals may be observed provided the γ -ray and neutrino beams intersect the direction to the Earth, or sweep across the Earth giving rise to a pulsed signal. For a beaming solid angle of Ω_b steradians, the prompt neutrino flux may be calculated from

$$F_\nu(E_\nu) \approx \frac{\dot{N}_{\text{Fe}}}{\Omega_b d^2} [1 - \exp(-\tau_{pp})] \int N_n(E_n) P_{n\nu}^M(E_\nu, E_n) dE_n \quad (13)$$

where d is the distance to the SNR, and $P_{n\nu}^M(E_\nu, E_n) dE_\nu$ is the number of neutrinos produced with energies in the range E_ν to $(E_\nu + dE_\nu)$ (via pion production and subsequent decays) in multiple nucleon-nucleon interactions of a nucleon of energy E_n . Nucleon-nucleon interactions were treated as described in [43] and the pions produced were decayed using SIBYLL [44]. All the results given below are for $\Omega_b = 1$ sr, and for smaller beams the fluxes should therefore be scaled up by a factor Ω_b^{-1} .

In the case of γ -ray production, a significant fraction of the γ -rays will interact by pair production with target nuclei in the shell and will not be observed. Also, during the first few months, TeV γ -rays could interact with radiation from the photosphere of the supernova [45]. By several days after the explosion, the radius of the photosphere becomes smaller than that of the SNR shell, where the neutrons interact, and continues to decrease in radius relative to the shell. Thus, interactions with radiation from the photosphere is likely to be a small effect here as the γ -rays will be travelling in the directions of their parent neutrons, i.e. radially outwards from the neutron star, and the angle between the directions of the γ -rays and soft photons from the photosphere will be small, reducing the interaction probability. Concentrating on pair production with matter, the optical depth of the shell is determined by the mean free path for pair production which at high energies is $(9/7)$ of the radiation length, giving $\tau_{\gamma p} \approx 0.7\tau_{pp}$. For a neutron interacting at some fraction, f , of the way through the shell, a γ -ray produced at that point would have a probability of $\exp[-(1-f)\tau_{\gamma p}]$ of escaping from the shell. Integrating over neutron interaction points (γ -ray emission points) within the shell we arrive at the prompt gamma ray flux at Earth,

$$F_\gamma(E_\gamma) \approx \frac{\dot{N}_{\text{Fe}}}{\Omega_b d^2} \frac{\exp(-\tau_{pp}) - \exp(-\tau_{\gamma p})}{(\tau_{\gamma p}/\tau_{pp}) - 1} \int N_n(E_n) P_{n\gamma}^M(E_\gamma, E_n) dE_n, \quad (14)$$

where $P_{n\gamma}^M(E_\gamma, E_n) dE_\gamma$ is the number of γ -rays produced with energies in the range E_γ to $(E_\gamma + dE_\gamma)$ (via pion production and subsequent decays) by multiple nucleon-nucleon interactions of a nucleon of energy E_n . Note that this neglects cascading in the matter as a result of bremsstrahlung and subsequent pair production, and so the prompt γ -ray flux at low energies will be somewhat underestimated.

Light curves for prompt neutrinos above 1 TeV, and γ -rays above 100 MeV and 1 TeV, are shown for $B \sin i = 10^{13}$ G in Fig. 8(a) for $P_0 = 5$ ms and in Fig. 8(b) for $P_0 = 2$ ms.

The results are shown here, and in the remaining figures, for a distance of $d = 10$ kpc. In both cases, results are given for three radiation field models (no polar cap heating, moderate polar cap heating, and maximum polar cap heating), and the pulsar period and the surface and polar cap temperatures vary appropriately with time after the explosion. In Fig. 9(a) we show the energy spectrum of prompt γ -rays, and in Fig. 9(b) the energy spectrum of prompt neutrinos, both at $t = 0.1$ year for each initial period and radiation field model. In Fig. 10 we show how the energy spectrum of prompt neutrinos evolves with time for the case of $P_0 = 5$ ms and the maximum polar cap heating model. In both Figs. 9(b) and 10 we show the atmospheric neutrino background flux within 1° and within 10° of the source direction based on the intensity calculated by Lipari [46].

5.2 Delayed gamma-ray and neutrino spectra

At later times, when τ_{pp} is not too large, the neutrons can travel through the SNR shell without significant losses and subsequently decay outside of the shell. The protons from neutron decay will be trapped to some extent and isotropized by ambient magnetic fields, and so will await the arrival of a dense matter target in the form of the SNR shell before having any significant probability of interacting. We make the approximation that the trapping is complete, i.e. that a proton does not diffuse far from where its parent neutron decayed during the time it takes the SNR shell to reach the proton. For the present assumptions, energy in the form of energetic protons is then, in effect, stored outside the shell and has contributions from neutrons produced at all times from $t = 0$ to the time of observation, t .

The number density per unit energy, at energy E_n , of neutrons at radius r and time t is

$$n_n(E_n, r, t) \approx \frac{\exp(-r/\gamma_n \tau_n c)}{4\pi r^2 c} \dot{N}_n(E_n, t) [1 - \exp(-\tau_{pp}(t))], \quad (15)$$

where $\tau_n \approx 890$ s is the neutron decay time, and $\gamma_n = E_n/m_n c^2$ is the Lorentz factor of the neutrons, \dot{N}_n is given by Eq. 11, and we neglect the travel time of relativistic particles. The net rate of production of protons per unit energy by neutron decay, at energy E_n , per unit volume at radius r and time t is then simply

$$\dot{n}_p(E_p, r, t) \approx n_n(E_p, r, t) / (\gamma_p \tau_n) \quad (16)$$

where we make the approximation that in neutron decay $E_p \approx E_n$ ($\gamma_p \approx \gamma_n$), and that losses of protons can be neglected. Then, integrating over the age of the supernova we obtain the number density per unit energy, at energy E_p , of protons at radius r and time t

$$\begin{aligned} n_p(E_p, r, t) &\approx \int_0^t \dot{n}_p(E_p, r, t') dt' \\ &\approx \frac{\exp(-r/\gamma_p \tau_n c)}{4\pi r^2 \gamma_p \tau_n c} \int_0^t \dot{N}_n(E_p, t') [1 - \exp(-\tau_{pp}(t'))] dt'. \end{aligned} \quad (17)$$

At time t , we make the approximation that the bulk of the matter in the SNR shell is located near radius $r = v_{\text{SN}} t$ within a shell of volume $V = 4\pi r^2 \Delta$ where Δ is the shell thickness and $\Delta \ll r$, so that the number density of target nucleons experienced by stored energetic protons interacting at time t is $n_H(t) \approx M_{\text{SN}}/(V m_p)$. Thus we obtain the rate at which an individual stored energetic proton interacts, $n_H(t) \sigma_{pp} c$, and from this one can obtain the total number of protons per unit energy, at energy E_p , interacting per unit time at supernova age t by simply integrating over the interaction volume,

$$\dot{N}_p(E_p, t) \approx \frac{\sigma_{pp} M_{\text{SN}}}{m_p} \frac{\exp(-v_{\text{SN}} t / \gamma_p \tau_n c)}{4\pi v_{\text{SN}}^2 t^2 \gamma_p \tau_n} \int_0^t \dot{N}_n(E_p, t') [1 - \exp(-\tau_{pp}(t'))] dt'. \quad (18)$$

It is now relatively straightforward to calculate the delayed neutrino and γ -ray fluxes. The delayed neutrino flux is given by

$$F_\nu(E_\nu, t) \approx \frac{1}{4\pi d^2} \int \dot{N}_p(E_p, t) P_{p\nu}^S(E_\nu, E_p) dE_p, \quad (19)$$

and the delayed γ -ray flux is given by

$$F_\gamma(E_\gamma, t) \approx \frac{[1 - \exp(-\tau_{\gamma p}(t))]}{4\pi d^2 \tau_{\gamma p}(t)} \int \dot{N}_p(E_p, t) P_{p\gamma}^S(E_\gamma, E_p) dE_p, \quad (20)$$

where the extra factors involving $\tau_{\gamma p}$ arise from the solution of the equation of radiative transfer for the case of uniform emission in a slab of optical depth $\tau_{\gamma p}$, and $P_{p\nu}^S(E_\nu, E_p) dE_\nu$ is the number of neutrinos produced with energies in the range E_ν to $(E_\nu + dE_\nu)$ (via pion production and subsequent decays) in a single nucleon-nucleon interaction of a nucleon of energy E_p , and $P_{p\gamma}^S(E_\gamma, E_p)$ is defined similarly.

Light curves for delayed neutrinos above 1 TeV, and γ -rays above 100 MeV and 1 TeV, are shown for $B \sin i = 10^{13}$ G in Fig. 11(a) for $P_0 = 5$ ms and in Fig. 11(b) for $P_0 = 2$ ms. In each case, results are shown for three radiation field models and we vary the pulsar period and surface temperatures appropriately with time after the explosion. In the case of the TeV γ -ray light curve, a minor additional attenuation of γ -rays in the radiation field of the SN photosphere [45] has been included as the γ -ray emission is isotropic (the interacting protons having been isotropized) and the angles between interacting photons will typically be larger than in the case of prompt gamma rays. Nevertheless, this is a relatively small effect on the delayed spectrum as $\sim 90\%$ of TeV γ -rays are unaffected by photon-photon pair production after $t = 100$ days [45]. In Fig. 12(a) we show the energy spectrum of delayed γ -rays (neglecting attenuation of γ -rays in the radiation field of the SN photosphere), and in Fig. 12(b) the energy spectrum of delayed neutrinos, both at $t = 1$ year and for each initial period and radiation field model. In Fig. 12(b) we also show the atmospheric neutrino background flux within 1° and within 10° of the source direction based on the intensity calculated by Lipari [46].

6 Discussion and Conclusion

We first discuss some of the limitations of our calculations. Perhaps the least justifiable approximation is our assumption that the ejected matter is contained in a *thin* SNR shell. Other approximations we have made include assuming that delayed signals produced simultaneously anywhere in the SNR shell arrive simultaneously at Earth, and that protons from neutron decay do not diffuse far during the time it takes the SNR shell to reach them. The main effect of including a more realistic density profile in the shell, and also taking account of travel-time delays of signals arriving from different parts of the shell, would be to smear out in time the light curve of the delayed signals we predict by $\sim r_{\text{SN}}/c = \beta_{\text{SN}}$. Looking at the light-curves of delayed signals given in Fig. 11, we note that for $\beta_{\text{SN}} = 0.03$ the effect of smearing of the light-curve by these effects will be minimal. For the third assumption, that protons do not diffuse far from neutron decay sites, the main effect of including diffusion will also be to smear out the light-curve of delayed signals. However, the diffusion coefficient is rather uncertain and strongly energy dependent, being small at low energies. The effect will be minimal at 100 MeV energies, but could be important for delayed TeV γ -ray and neutrino signals.

We have also neglected any signals arising from the protons extracted from Fe-nuclei, and also signals from nuclei that were not completely fragmented into nucleons in the radiation field of the pulsar. We assume these particles, being charged, will be trapped in the central region of the SNR where the matter density is expected to be relatively low, and would not contribute significantly to the γ -ray and neutrino fluxes. These nuclei would be subject to adiabatic deceleration as the SNR expands. However, some would accumulate and eventually contribute to the galactic cosmic rays towards the end of the SNR's life.

We next discuss whether the signals we predict from young SNR are observable with existing and planned experiments (see e.g. ref. [47] for a summary of γ -ray detector thresholds). The prompt γ -ray light curve peaks at about 2 months after the explosion (see Fig. 8). The peak flux above 100 MeV for a pulsar at 10 kpc with $B \sin i = 10^{13}$ G ranges from $2 \times 10^{-6} \text{ cm}^{-2} \text{ s}^{-1}$ ($P_0 = 5$ ms, no polar cap heating) to $1.5 \times 10^{-4} \text{ cm}^{-2} \text{ s}^{-1}$ ($P_0 = 2$ ms, maximum polar cap heating) if $\xi \Omega_b^{-1} = 1 \text{ sr}^{-1}$. The sensitivity of the EGRET detector on the Compton Gamma Ray Observatory for 100 MeV γ -rays is $\sim 7 \times 10^{-8} \text{ cm}^{-2} \text{ s}^{-1}$, and with this sensitivity prompt γ -rays from a Galactic source should easily be detected for several months if a significant fraction of the electromagnetic power goes into accelerating heavy nuclei and the pulsar's γ -ray beam sweeps across the Earth. With future 100 MeV γ -ray detectors, even lower detection thresholds (e.g. $\sim 5 \times 10^{-9} \text{ cm}^{-2} \text{ s}^{-1}$ for GLAST) should enable more distant pulsars such as those in the Magellanic Clouds to be detected.

In the case of the delayed flux, the situation is less promising. The delayed γ -ray light curve peaks at about 6 months after the explosion (see Fig. 11). The peak flux above 100 MeV for a pulsar at 10 kpc with $B \sin i = 10^{13}$ G ranges from $3 \times 10^{-10} \text{ cm}^{-2} \text{ s}^{-1}$ ($P_0 = 5$ ms, no polar cap heating) to $1.2 \times 10^{-7} \text{ cm}^{-2} \text{ s}^{-1}$ ($P_0 = 2$ ms, maximum polar

cap heating) if $\xi = \xi_{\max} \approx 0.29$. In the three most optimistic cases (maximum polar cap heating with $P_0 = 2$ ms and $P_0 = 5$ ms, and moderate heating and $P_0 = 2$ ms), detection by EGRET should be possible provided ξ is sufficiently high. With GLAST detection should be possible for both initial periods and both maximum and moderate polar cap heating provided ξ is sufficiently high.

The current generation of Cherenkov telescopes operating at TeV energies (e.g. the Whipple Observatory, and the CANGAROO telescope [48]) have thresholds of a few $\times 10^{-12} \text{ cm}^{-2} \text{ s}^{-1}$, and GRANITE III (Whipple telescope with new camera) is expected to have a threshold of $\sim 10^{-12} \text{ cm}^{-2} \text{ s}^{-1}$. For Galactic sources, the predicted prompt TeV fluxes (see Fig. 8) are well above this threshold and should easily be detected even for the least optimistic case ($P_0 = 5$ ms, no polar cap heating) provided $\xi \Omega_b^{-1} > 10^{-4} \text{ sr}^{-1}$, for the most optimistic case ($P_0 = 2$ ms, maximum polar cap heating) provided $\xi \Omega_b^{-1} > 10^{-6} \text{ sr}^{-1}$. In the case of delayed γ -rays (see Fig. 11), it should be possible to observe a galactic source for up to a few years depending on ξ . With the sensitivity of current TeV γ -ray telescopes, it should be possible to detect prompt γ -rays from sources in the Magellanic Clouds, and we shall discuss below constraints placed on our model by the non-detection of γ -rays from SN 1987A.

Available upper limits on the TeV γ -ray flux from SN 1987A are as follows: $t \approx 10$ months (November 1987) — $2.3 \times 10^{-11} \text{ cm}^{-2} \text{ s}^{-1}$ above 1 TeV (Raubenheimer et al. [12]); $t \approx 1$ year — $6.1 \times 10^{-12} \text{ cm}^{-2}$ above 3 TeV (Bond et al. [8]); $t \approx 1$ year (January/February 1988) — $1.6 \times 10^{-10} \text{ cm}^{-2} \text{ s}^{-1}$ above 0.4 TeV (Chadwick et al. [10]). Assuming a distance of 55 kpc, comparison of the predicted delayed γ -ray fluxes with the observed upper limit at 1 TeV (Raubenheimer et al. [12]) allows us to place constraints on ξ . In the case of maximum polar cap heating (see Fig. 11b) the limit is $\xi < 0.15$ if the initial pulsar period is $P_0 = 2$ ms, and $\xi < 0.4$ for $P_0 = 5$ ms. For moderate polar cap heating and $P_0 = 2$ ms, $\xi < 0.25$. The value of ξ for other models is not constrained by the observations because the predictions for $\xi = \xi_{\max}$ are below the reported upper limits. The prompt γ -ray fluxes are significantly higher than the delayed fluxes, but they depend also on the solid angle for beaming, Ω_b . If the observer is inside the beam of energetic neutrons injected by the pulsar, which will also define the prompt γ -ray beam, then the value of $\xi \Omega_b^{-1}$ can be constrained by the upper limit mentioned above, giving $\xi \Omega_b^{-1} < 7 \times 10^{-3} \text{ sr}^{-1}$ for the case of $P_0 = 2$ ms (see Fig. 8b). However, we note that since no pulsar has yet been discovered inside SN 1987A this could be interpreted as suggesting that we are outside the beam of the neutron injection.

The technique for constructing a large area (in excess of 10^4 m^2) neutrino telescope has been known for more than a decade [49]. In pioneering work, the DUMAND Collaboration developed techniques to instrument a large volume of water in a deep ocean trench with strings of photomultipliers to detect Cherenkov light from neutrino-induced muons. Locations deep in the ocean shield the detectors from cosmic ray muons. The DUMAND detector [50] was designed to be most sensitive to neutrinos above about 1 TeV, and prototypes of other similar experiments are already in operation such as that in Lake Baikal, Siberia [51], and NESTOR off the coast of Greece [52]. An exciting recent

development has been the construction of a DUMAND type detector deep in the polar ice cap at the South Pole. This experiment called AMANDA uses the same principle as DUMAND but takes advantage of excellent transparency of the polar ice under extreme pressures and a stable environment in which to embed the detectors [53]. These experiments which operate typically above 1 TeV have the potential to be expanded in the future to a detector on the 1 km^3 scale. The background to these experiments at 1 TeV is due primarily to atmospheric neutrinos, but at higher energies there is an uncertain background of prompt muons from charm production (see e.g. Gaisser et al. [54] for a discussion). For recent reviews of the predicted intensity of diffuse high energy neutrinos of astrophysical origin see refs. [54, 55].

Referring to Figs. 9(b) and 10 we see that for good angular resolution (1°) the prompt neutrino flux above 1 TeV is well above the atmospheric background, and even for 10° resolution the prompt neutrino signal should be observed. However, observation of any prompt signal would require the neutrino beam (essentially the beam of the primary neutrons) to sweep across the Earth. Because of this uncertain beaming, the situation may actually be more promising for delayed neutrinos (Fig. 12b). For 1° resolution and $\xi\Omega_b^{-1} = 1 \text{ sr}^{-1}$, TeV neutrinos should be easily observable for the case of hot polar caps, but detection would be marginal for the case of no polar cap heating. With 10° resolution detection of galactic sources would be marginal even in the most optimistic scenario except for the case of extremely large detectors, e.g. km^3 [56], which with large statistics could see a weak signal significantly below the atmospheric background. A large detector with excellent angular resolution would be required to observe very young SNR in the Magellanic Clouds unless the emission were beamed towards the Earth.

In Conclusion, we have considered a model for γ -ray and neutrino emission by very young supernova remnants in which ions are accelerated in the slot gap of a highly magnetized rapidly spinning pulsar. Energetic neutrons are extracted from the ions by photodisintegration during interactions with thermal radiation from the neutron star surface and hot polar caps. Prompt gamma ray and neutrino signals are produced by energetic neutrons interacting with target nuclei as they travel out through the SNR shell. Delayed γ -ray and neutrino signals are produced by energetic protons from the decay of neutrons which have passed through the SNR shell. These protons diffuse slowly from where the neutrons decayed, and interact with target nuclei when the SNR shell catches up with them. For a limited range of pulsar parameters these signals should be observable from very young SNR in our Galaxy with existing and planned γ -ray and neutrino telescopes.

Acknowledgements

W.B. thanks the Department of Physics and Mathematical Physics at the University of Adelaide for hospitality during his visit. Q.L. acknowledges receipt of an Australian Research Council (ARC) Postdoctoral Fellowship. This research is supported by a grant from the ARC.

References

- [1] Berezinsky, V.S., and Prilutsky, O.F., *Astron. Astrophys.* **66** (1978) 325.
- [2] Sato, H., *Prog. Theor. Phys.* **58** (1978) 549.
- [3] Gaisser, T.K., Harding, A.K., Stanev, T., *Nature* **329** (1987) 314.
- [4] Gaisser, T.K., Harding, A.K., and Stanev, T., *Ap.J.* **345** (1989) 423.
- [5] Yamada, Y., Nakamura, T., Kasahara, K., and Sato, H., *Prog. Theor. Phys.* **79** (1987) 426.
- [6] Berezinsky, V.S., and Ptuskin, V.S., *Astron. Astrophys.* **215** (1989) 339.
- [7] Bond, I.A. et al. *Phys. Rev. Lett.* **60** (1988) 1110.
- [8] Bond, I.A. et al. *Phys. Rev. Lett.* **61** (1988) 2292.
- [9] Bond, I.A. *Ap.J.* **344** (1989) L17.
- [10] Chadwick, P.M., et al. *Ap.J.* **333** (1988) L19.
- [11] Ciampa, D. et al. *Ap.J.* **326** (1988) L9.
- [12] Raubenheimer, B.C. et al. *Astron. Astrophys.* **193** (1988) L11.
- [13] Allen, W.H. et al. *Phys. Rev. D* **48** (1993) 466.
- [14] van Stekelenborg, J. et al. *Phys. Rev. D* **48** (1993) 4504.
- [15] Rees, M.J., Gunn, J.E., *Mon. Not. R. Astron. Soc.* **167** (1974) 1.
- [16] Berezinsky, V.S., Ginzburg, V.L., *Nature* **329** (1987) 807.
- [17] Harding, A.K., Mastichiadis, A., Protheroe, R.J., Szabo, P., *Ap.J.* **378** (1991) 163.
- [18] Kirk, J.G., Duffy, P., Ball, L., *Astron. Astrophys.* **293** (1995) L37.
- [19] Hoshino, M., Arons, J., Gallant, Y.A., Langdon, A.B., *Ap.J.* **390** (1992) 454.
- [20] Gallant, Y.A., Arons, J., *Ap.J.* **435** (1994) 230.
- [21] Finley, J.P., Ögelman, H., Kiziloglu, Ü., *Ap.J.* **394** (1992) L21.
- [22] Halpern, J.P., Ruderman, M., *Ap.J.* **415** (1993) 286.
- [23] Ögelman, H., Finley, J.P., Zimmermann, H.U., *Nature* **361** (1993) 136.
- [24] Nomoto, K., Tsuruta, S., *Ap.J.* **312** (1987) 711.

[25] Ögelman, H., *Neutron stars: Theory and Observation*, J. Ventura & D. Pines (eds.), (Kluwer), 87.

[26] Ruderman, M., Sutherland, P.G. *Ap.J.* **196** (1975) 51.

[27] Arons, J., Scharlemann, E.T., *Ap.J.* **231** (1979) 854.

[28] Helfand, D.J., Chanan, G.A., Novick, R., *Nature* **283** (1980) 337.

[29] Cheng, K.S., Ho, C., Ruderman, M., *Ap.J.* **300** (1986) 500

[30] Cheng, K.S., Ho, C., Ruderman, M., *Ap.J.* **300** (1986) 522

[31] Bednarek, W., and Protheroe, R.J., in preparation.

[32] Bednarek, W., Karakuła, S., *Proc. 24th Int. Cos. Ray Conf.* (Rome) **2** (1995) 279.

[33] Karakuła, S., Tkaczyk, W., *Astropart.Phys.* **1** (1993) 229.

[34] Shapiro, S.L., and Teukolsky, S.L., *Black Holes, White Dwarfs and Neutron Stars* (New York: Wiley, 1983).

[35] Taylor, J.H., Manchester, R.N., Lyne, A.G. *ApJS* **88** (1993) 529

[36] Manchester, R.N., and Taylor, J.H., *Pulsars* (San Francisco: Freeman, 1977).

[37] Michel, F. C., *Ap.J.* **192** (1974) 713.

[38] Fawley, W. M., Arons, J. & Scharlemann, E. T., *Ap.J.* **217** (1977) 227.

[39] Rosen, L. C. & Cameron, A. G. W., *Astroph. & Space Sci.* **15** (1972) 137.

[40] Arons, J., *Ap.J.* **248** (1981) 1099.

[41] Arons, J., *Ap.J.* **266** (1983) 215.

[42] Luo, Q., Protheroe, R.J., & Bednarek, W., in preparation.

[43] Hillas, A.H., in *Proc. 17th Int'l Cosmic Ray Conf.* (Paris, 1981) **8**, p. 193.

[44] Fletcher R.S., Gaisser T.K., Lipari P., Stanev T. *Phys. Rev. D* **50** (1994) 5710.

[45] Protheroe, R.J., *Nature* **329** (1987) 135.

[46] Lipari, P., *Astroparticle Phys.* **1** (1993) 195.

[47] Sembroski, G., et al., 24th Int. Cos. Ray Conf. (Rome) **3** (1995) 428

[48] Hara, T., et al., *Nuclear Instr. & Methods in Phys. Res.* **A332** (1993) 300.

- [49] Berezinskii, V.S., and Zatsepin, G.T. *Sov. Phys. Usp.* **20** (1977) 361.
- [50] Learned, J.G., in “Frontiers of Neutrino Astrophysics”, eds. Y. Suzuki and K. Nakamura, (Universal Academy Press, Tokyo, 1993) p. 341.
- [51] Belolaptikov, I.A., *et al.*, in 24th Int. Cosmic Ray Conf. (Rome), **1** (1995) 742.
- [52] Capone, A., *et al.*, in 24th Int. Cosmic Ray Conf. (Rome), **1** (1995) 836.
- [53] Mock, P.C., *et al.*, in 24th Int. Cosmic Ray Conf. (Rome), **1** (1995) 758.
- [54] Gaisser, T.K., Halzen, F., and Stanev, T., *Phys. Rep.*, **258**, (1995) 173.
- [55] Protheroe, R.J., in *Towards the Millennium in Astrophysics: Problems and Prospects*, Erice 1996, eds. M.M. Shapiro and J.P. Wefel (World Scientific, Singapore), in press (1997) astro-ph/9612213
- [56] Halzen, F., Proc. Int. Symp. on Neutrino Telescopes, Venice, February 1996, in press, astro-ph/9605014

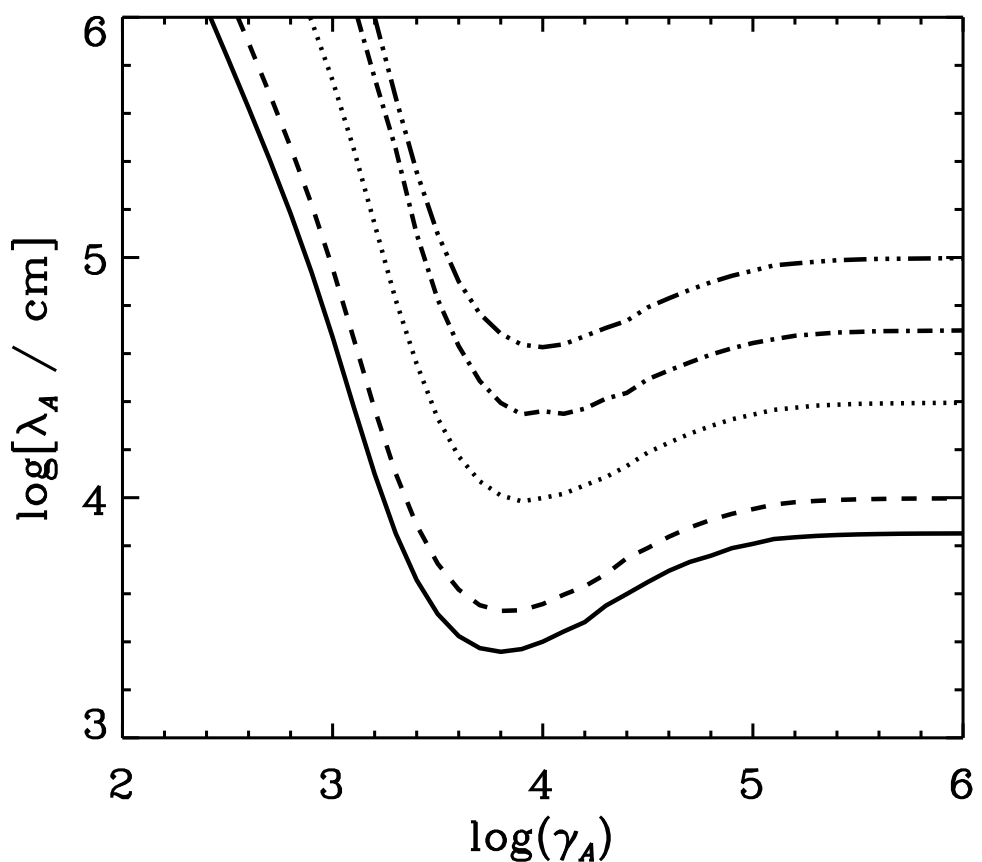


Figure 1: Mean free path for photodisintegration of nuclei in isotropic black body radiation at temperature $T = 10^7$ K as a function of Lorentz factor, γ_A , for various mass numbers A : 4 (top curve), 8, 16, 40, and 56 (bottom curve).

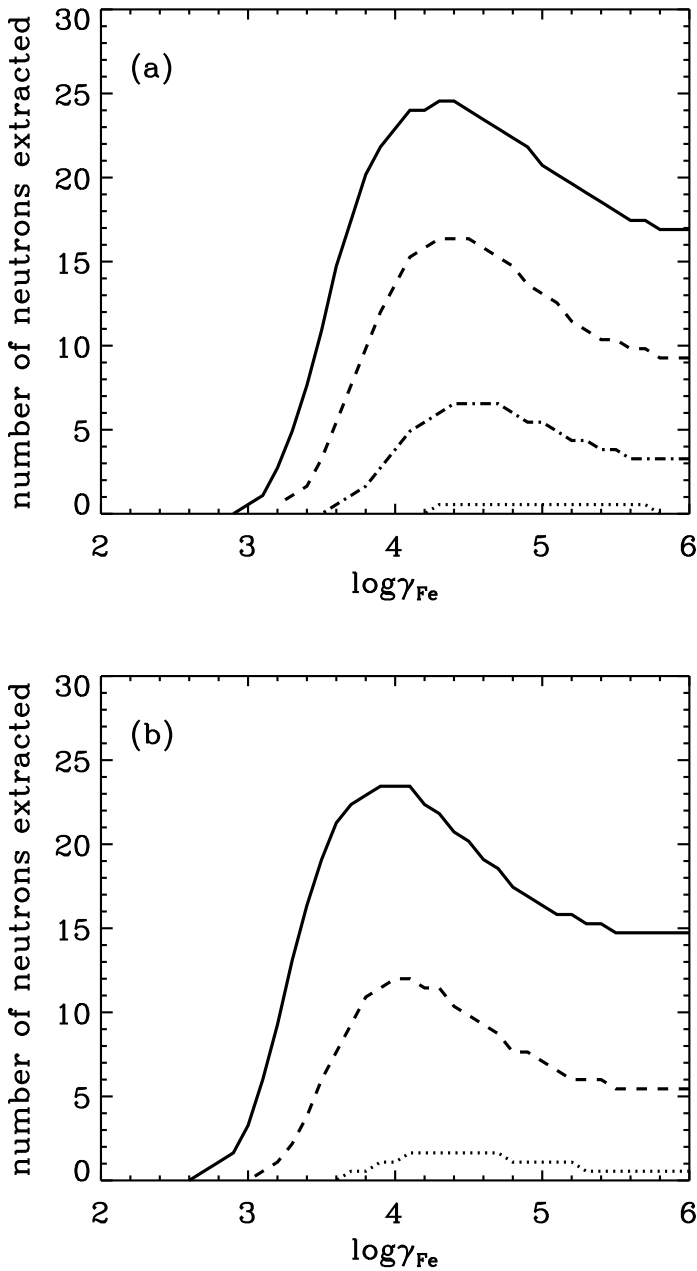


Figure 2: (a) Average number of neutrons extracted from a single Fe-nucleus during propagation along the neutron star's magnetic axis, from its surface at the pole to infinity, as a function of Lorentz factor. Neutron star spherical surface of radius 1.2×10^6 cm at constant temperature $T = 5 \times 10^6$ K (bottom curve), 10^7 K, 1.5×10^7 K, and 2×10^7 K (top curve). (b) Average number of neutrons extracted from a single Fe-nucleus during propagation along the neutron star's magnetic axis, from its surface at the pole to infinity, as a function of Lorentz factor, for field of heated polar cap of radius 10^5 cm with temperature $T = 10^7$ K (bottom curve), 2×10^7 K, and 3×10^7 K (top curve).

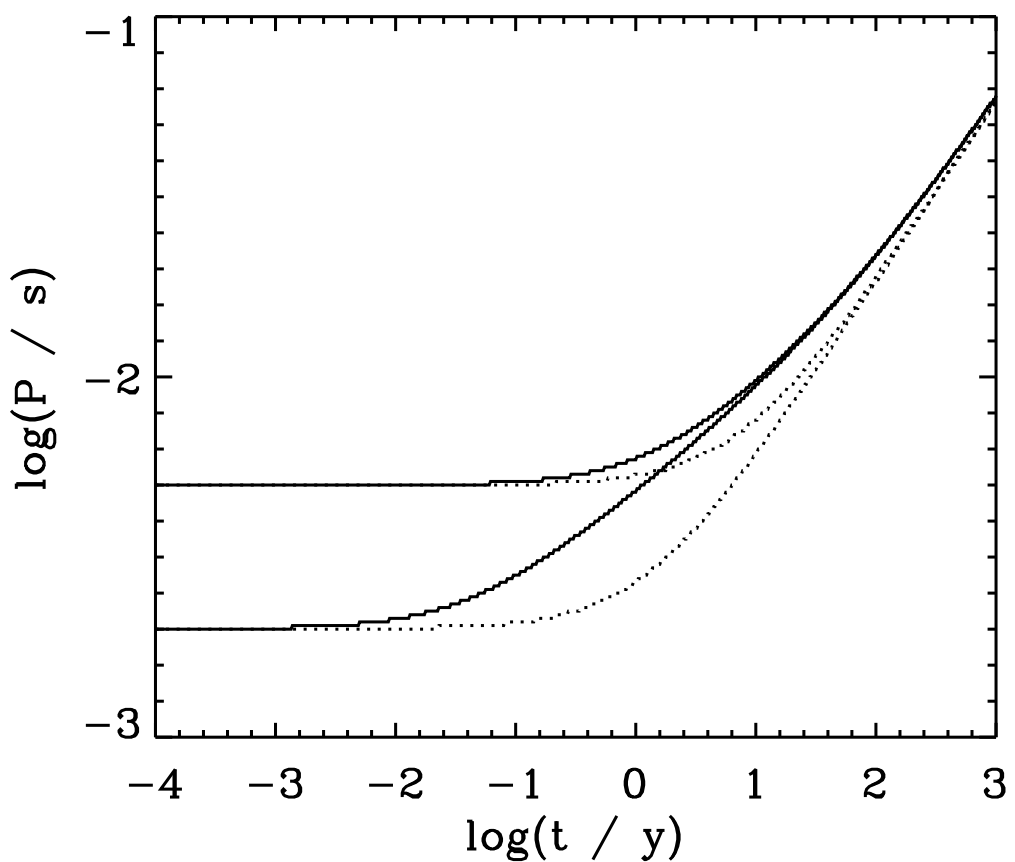


Figure 3: Evolution of pulsar period for $B \sin i = 10^{13}$ G for $P_0 = 0.002$ s (lower curves) and $P_0 = 0.005$ s (upper curves). Dotted curves are for electromagnetic radiation losses only, and solid curves include the effect of gravitational radiation losses.

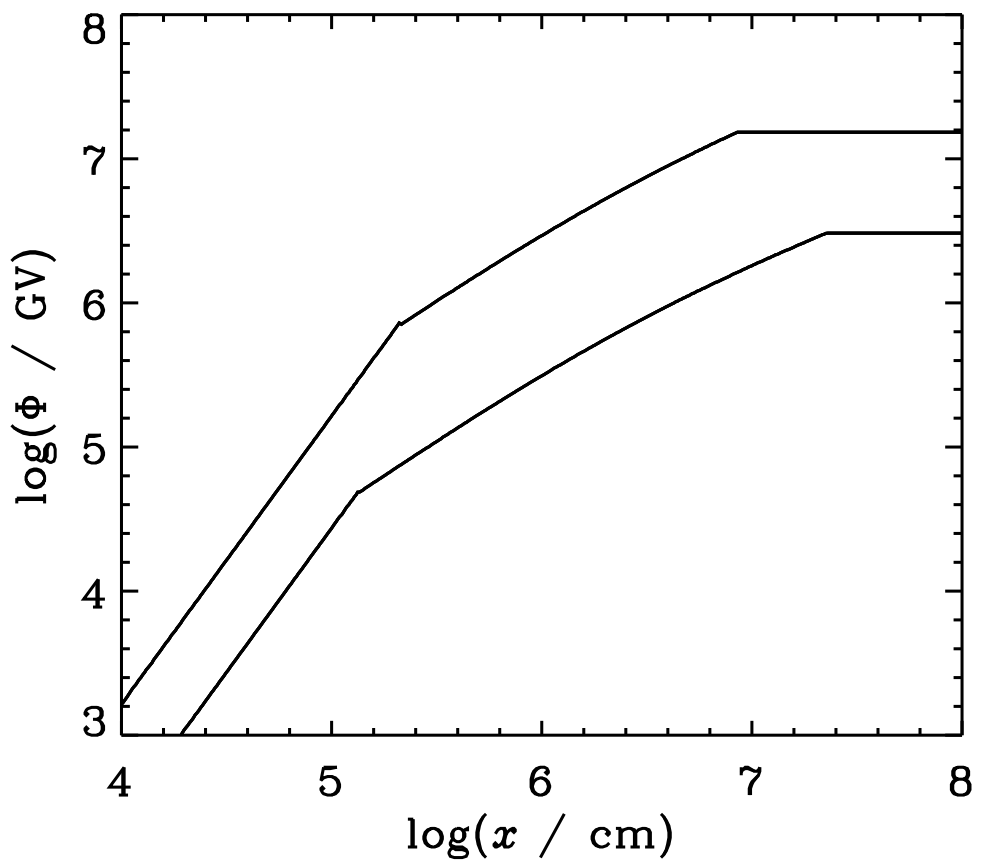


Figure 4: Slot gap potential given by Eq. 10 for $B = 10^{13} \text{ G}$ and $P = 0.005 \text{ s}$ (lower curve) and $P = 0.002 \text{ s}$ (upper curve). The potential is assumed constant for x larger than the light cylinder radius.

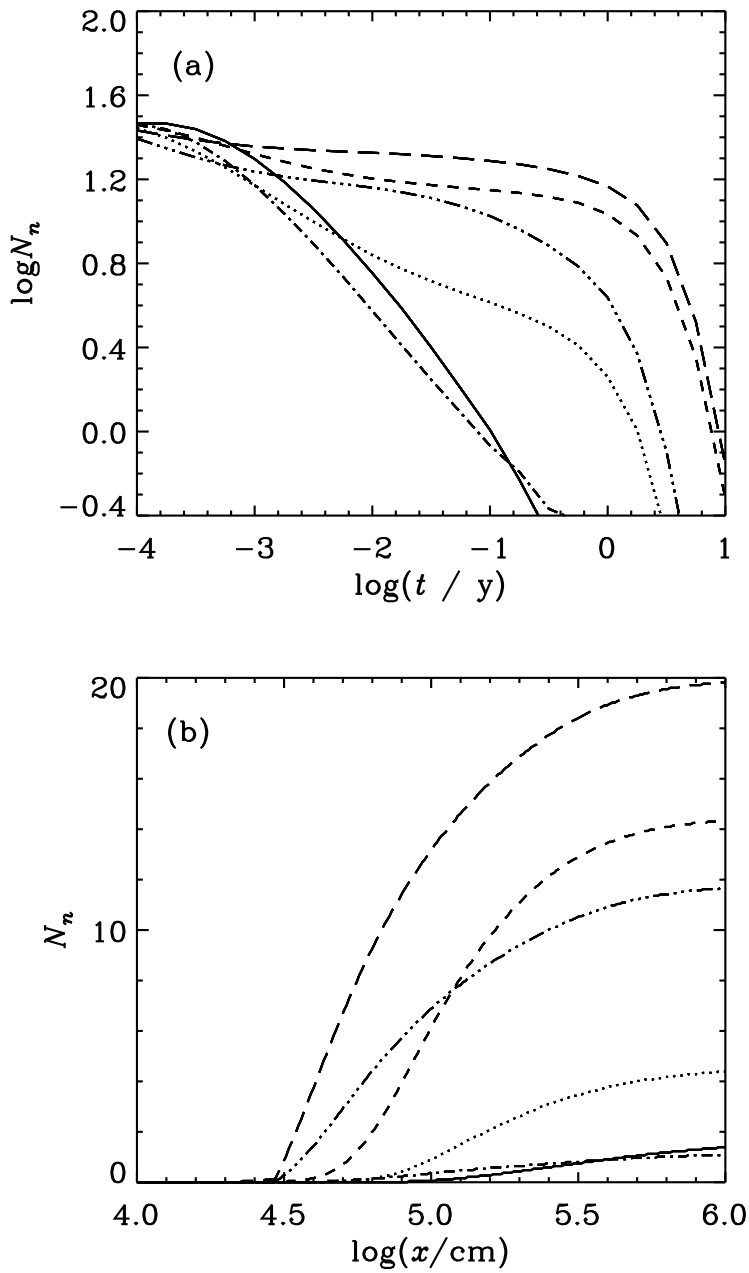


Figure 5: (b) Average cumulative number of neutrons extracted from a single Fe-nucleus during acceleration by the assumed slot gap potential for $B = 10^{13}$ G through the pulsar's radiation field as a function of neutron star neutron star age. (b) Average cumulative number of neutrons extracted from a single Fe-nucleus during acceleration at $t = 20.5$ days for 10^{13} G as a function of distance along the slot gap. Results are shown for the following (initial period, polar cap heating) configurations: $(P_0 = 5 \text{ ms, no polar cap heating})$ – solid curve; $(P_0 = 5 \text{ ms, moderate})$ – dotted curve; $(P_0 = 5 \text{ ms, maximum})$ – short-dashed curve; $(P_0 = 2 \text{ ms, no polar cap heating})$ – dot-dash curve; $(P_0 = 2 \text{ ms, moderate})$ – dot-dot-dot-dash curve; $(P_0 = 2 \text{ ms, maximum})$ – long-dashed curve.

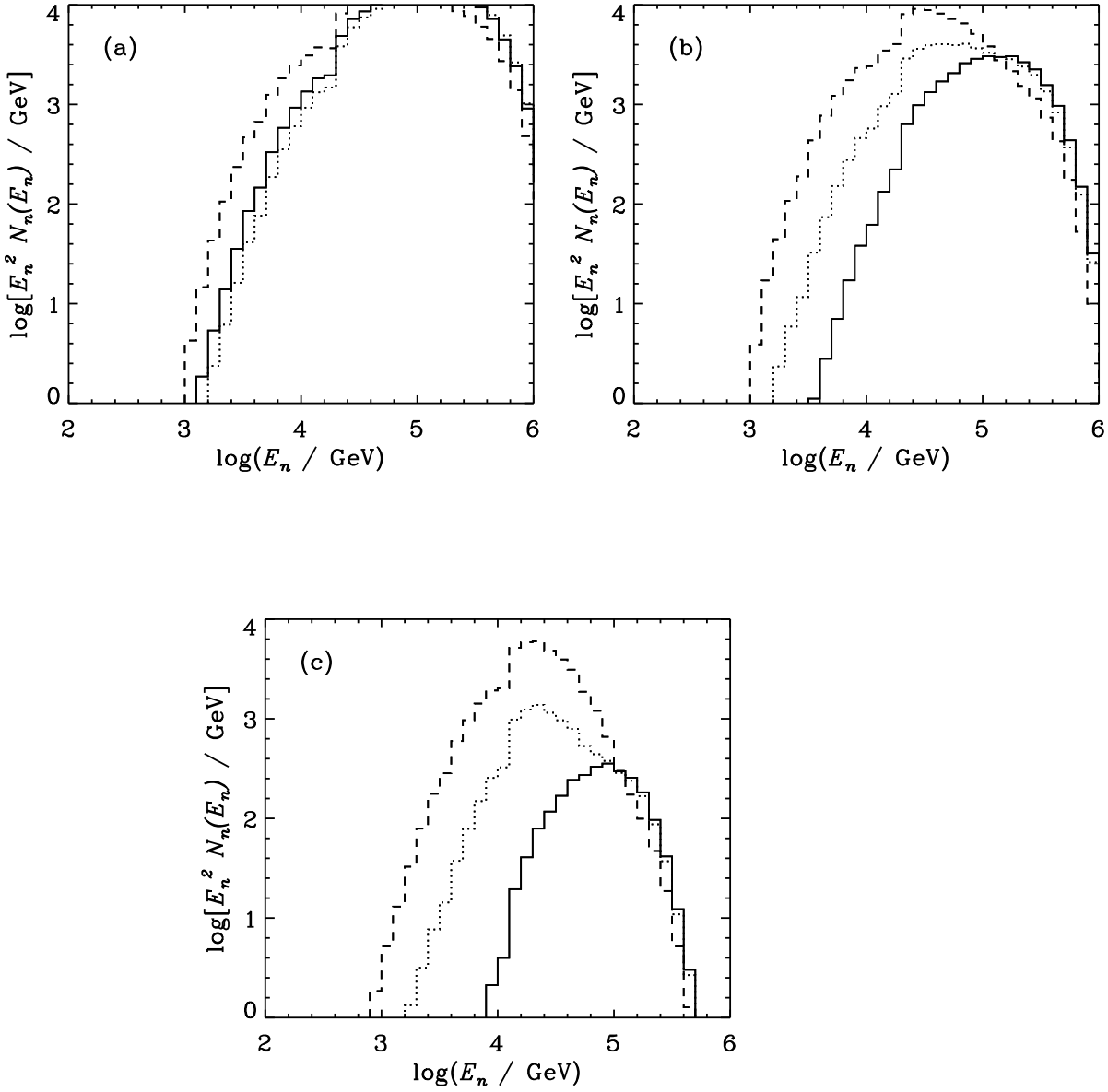


Figure 6: The spectrum of neutrons extracted from a single Fe-nucleus during acceleration for a pulsar with $P_0 = 5$ ms and $B = 10^{13}$ G at (a) $t = 1.15$ days ($P = 5.00$ ms), (b) $t = 20.5$ days ($P = 5.06$ ms), and (c) $t = 1$ year ($P = 5.94$ ms). Results are shown for the three radiation field models: no polar cap heating – solid histogram; moderate heating – dotted histogram; maximum heating – dashed histogram.

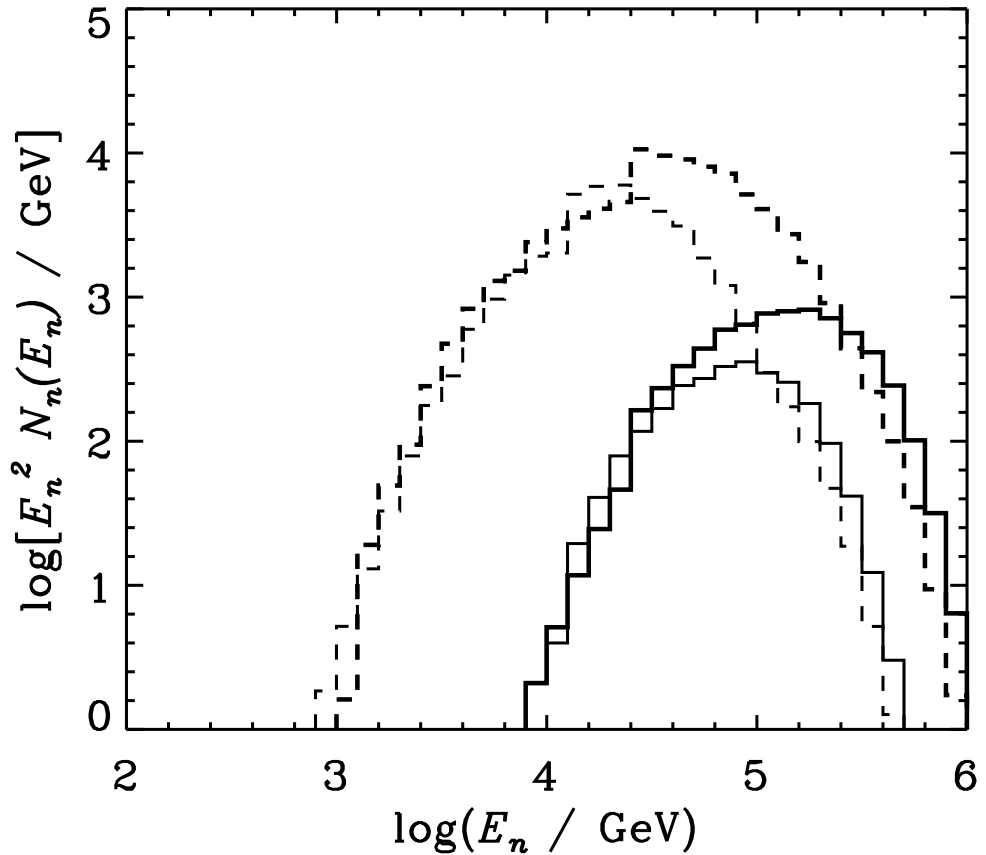


Figure 7: The spectrum of neutrons extracted from a single Fe-nucleus during acceleration at $t = 1$ year and $B = 10^{13}$ G for the following initial pulsar periods $P_0 = 5$ ms (thin histograms), and $P_0 = 2$ ms (thick histograms). Results are shown for two of the radiation field models: no polar cap heating – solid histograms; maximum heating – dashed histograms.

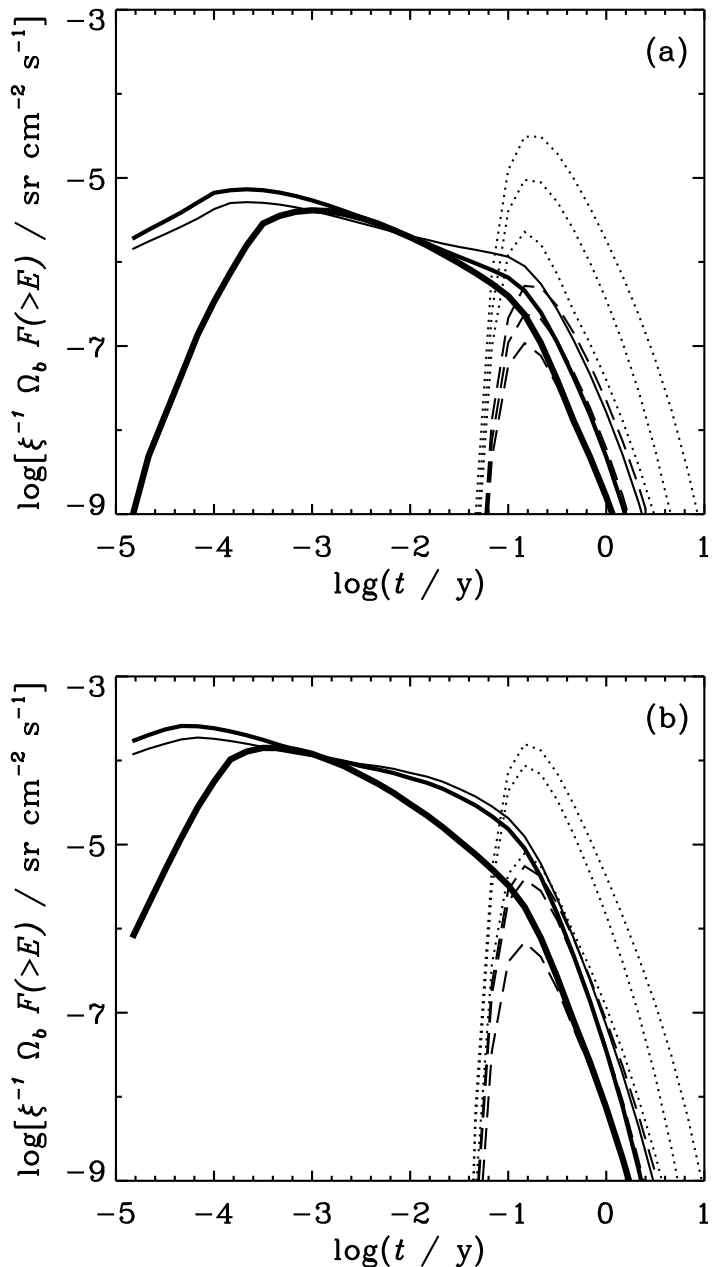


Figure 8: The dependence of the integral flux of prompt neutrinos ($\nu_\mu + \bar{\nu}_\mu$) above 1 TeV (solid curves), γ -rays above 100 MeV (dotted curves), and γ -rays above 1 TeV as a function of time t measured from the explosion for $d = 10$ kpc and $B = 10^{13}$ G and for (a) $P_0 = 5$ ms, and (b) $P_0 = 2$ ms. Results are shown for the three radiation field models: no polar cap heating – thickest solid curve and lowest dotted and dashed curves; moderate heating – middle curves; maximum heating – thinnest solid curve and upper dotted and dashed curves.

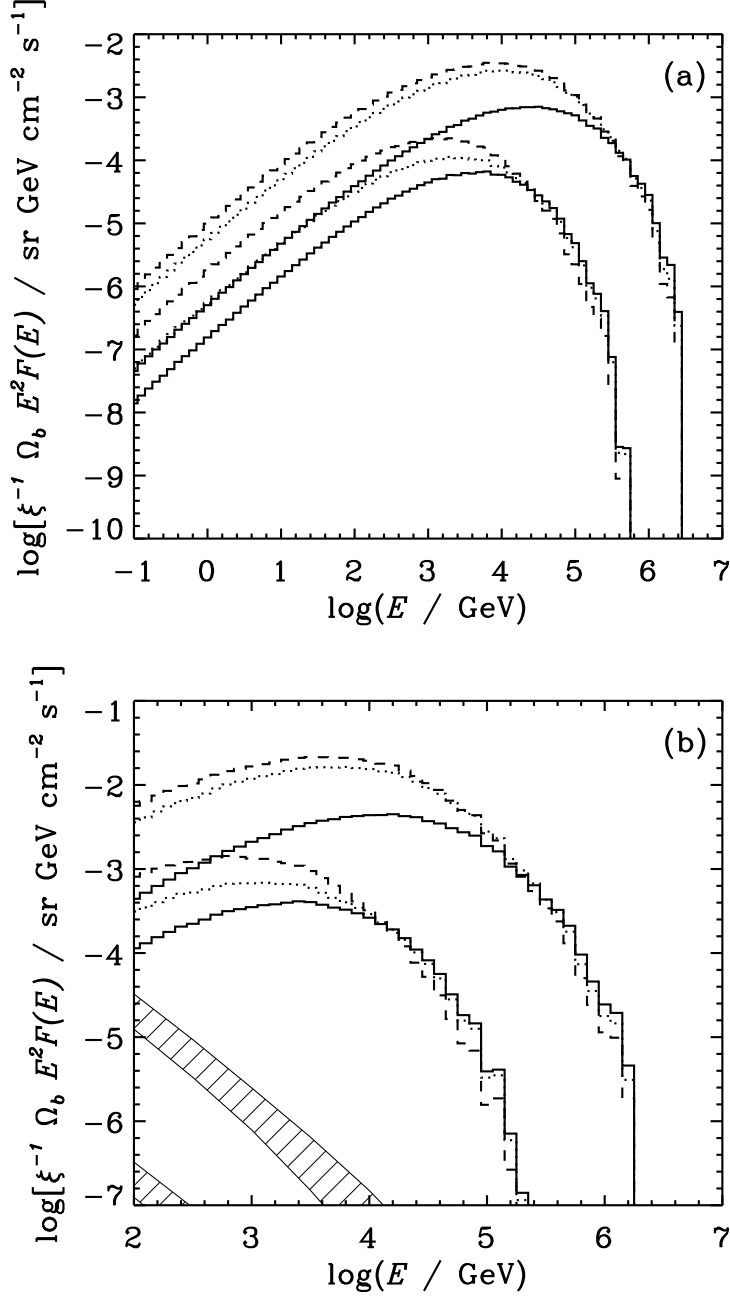


Figure 9: The spectra for $d = 10$ kpc at $t = 0.1$ year of (a) prompt γ -rays and (b) prompt neutrinos ($\nu_\mu + \bar{\nu}_\mu$) produced by collisions of neutrons with the matter of supernova shell. In each case, the upper three histograms are for $P_0 = 2$ ms, and the lower three histograms for $P_0 = 5$ ms. Results are shown for $B = 10^{13}$ G for the three radiation field models: no polar cap heating – lower histogram; moderate heating – middle histogram; maximum heating – upper histogram. The atmospheric neutrino background flux multiplied by E^2 ($\text{GeV cm}^{-2} \text{s}^{-1}$) within 1° and within 10° of the source direction, based on the intensity calculated by Lipari [46], is shown by the hatched bands (each band shows the range of atmospheric neutrino background as the zenith angle changes).

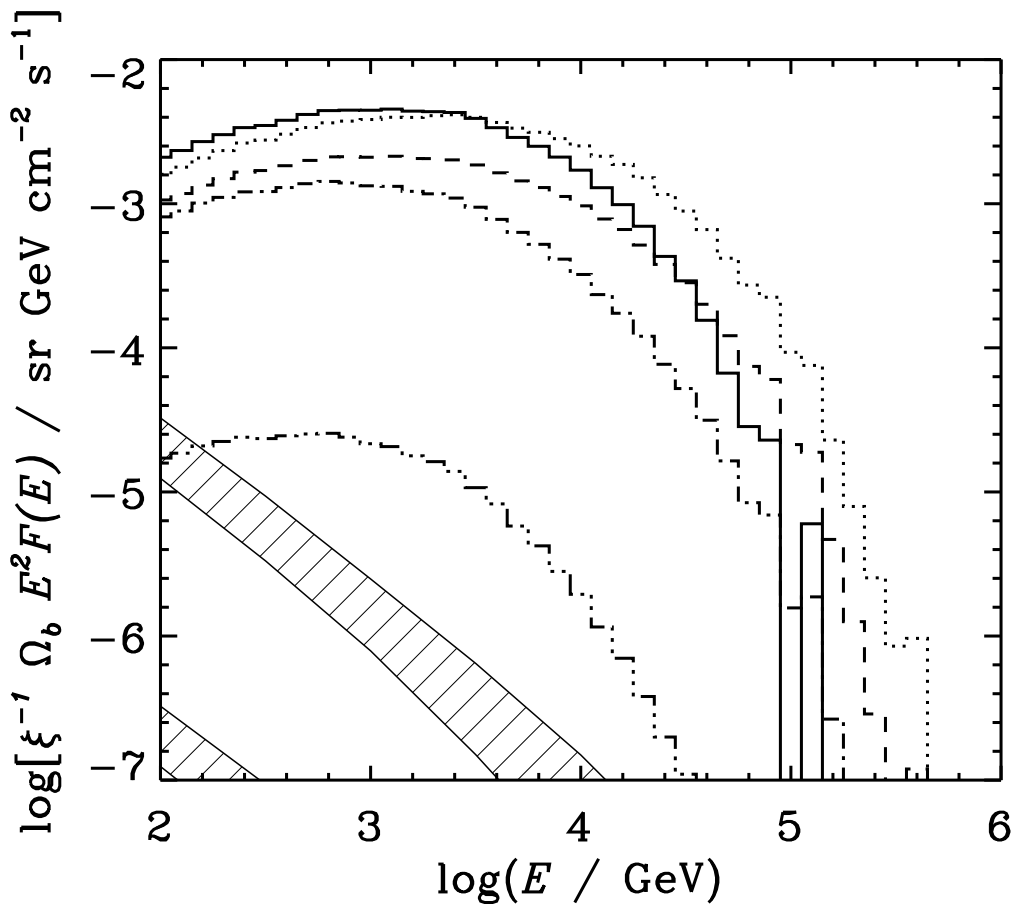


Figure 10: Evolution of the spectrum of prompt neutrinos ($\nu_\mu + \bar{\nu}_\mu$) produced by collisions of neutrons with matter in the supernova shell for $B = 10^{13}$ G, $P_0 = 5$ ms and the maximum polar cap heating model. Spectra are shown for $d = 10$ kpc and for $t = 10^{-4}$ y (solid histogram); 10^{-3} y (dotted histogram); 10^{-2} y (dashed histogram); 10^{-1} y (dot-dash histogram); 1 y (dot-dot-dot-dash histogram). See Fig. 9 for explanation of hatched bands.

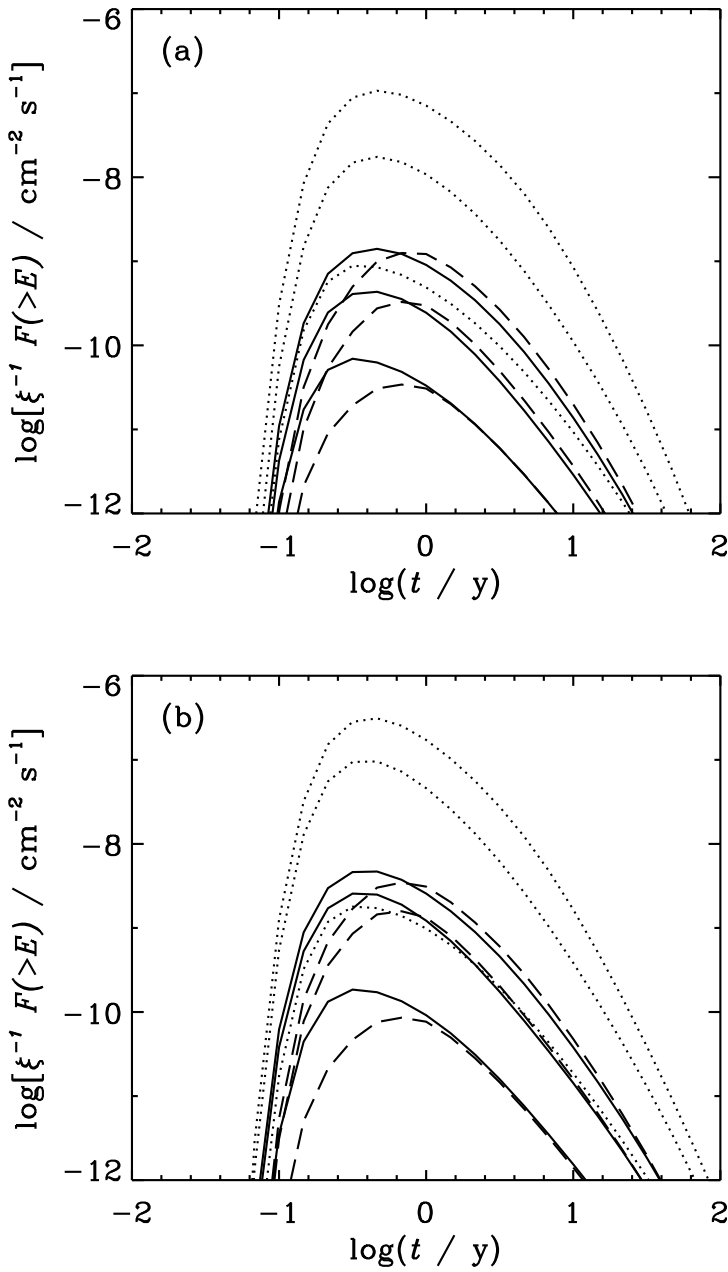


Figure 11: The dependence of the integral flux of delayed neutrinos ($\nu_\mu + \bar{\nu}_\mu$) above 1 TeV (solid curves), γ -rays above 100 MeV (dotted curves), and γ -rays above 1 TeV as a function of time t measured from the explosion for (a) $P_0 = 5$ ms, and (b) $P_0 = 2$ ms. Results are shown for $d = 10$ kpc, $B = 10^{13}$ G, and for the three radiation field models: no polar cap heating – lowest curves; moderate heating – middle curves; maximum heating – upper curves.

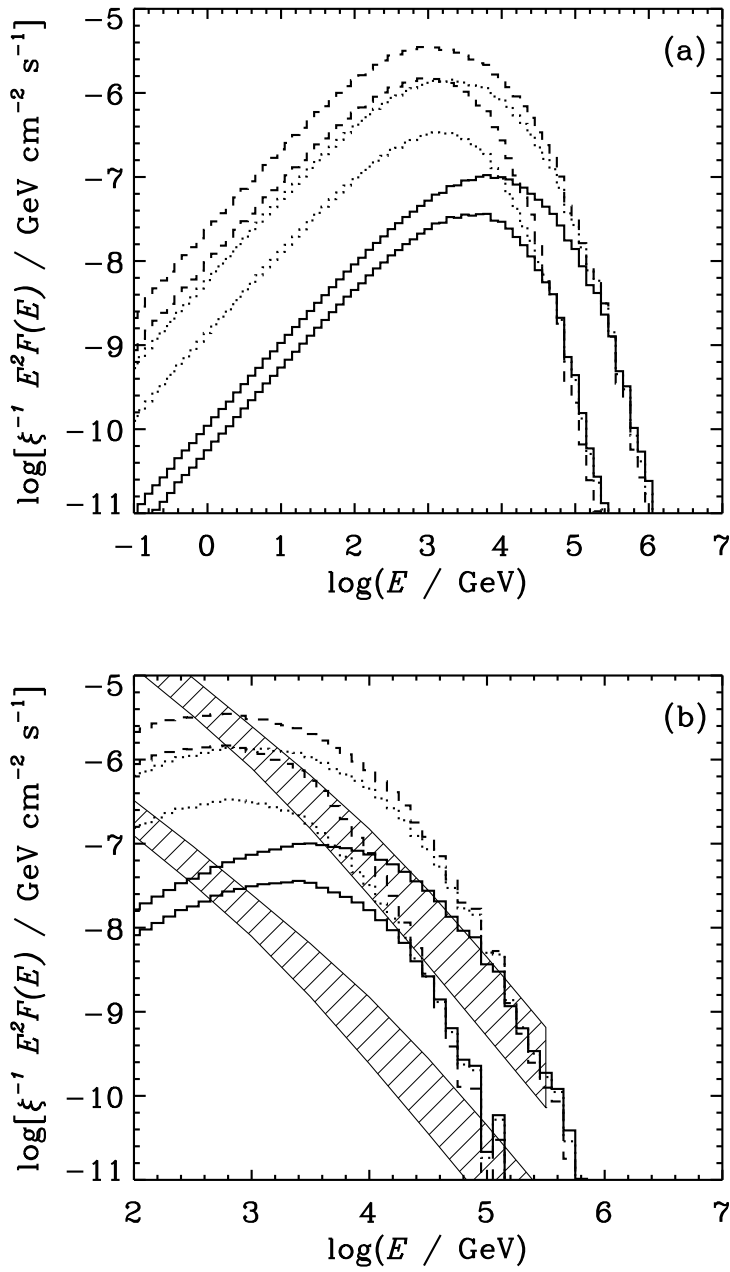


Figure 12: The spectra for $d = 10$ kpc and $B = 10^{13}$ G at $t = 1$ year of (a) delayed γ -rays and (b) delayed neutrinos ($\nu_\mu + \bar{\nu}_\mu$) produced by collisions of protons from neutron decay with matter in the supernova shell. See Fig. 9 for key to histograms. See Fig. 9 for explanation of hatched bands.